Nano Energy 83 (2021) 105847

Contents lists available at ScienceDirect

Nano Energy

journal homepage: http://www.elsevier.com/locate/nanoen

Revisiting the designing criteria of advanced solid electrolyte interphase on lithium metal anode under practical condition

Shouyi Yuan [a], Suting Weng [b], Fei Wang [e], Xiaoli Dong [a], Yonggang Wang [a], Zhaoxiang Wang [b], Cai Shen [d,*], Junwei Lucas Bao [c,*], Xuefeng Wang [b,f,**], Yongyao Xia [a,*]

[a] Department of Chemistry, Shanghai Key Laboratory of Catalysis and Innovative Materials, Center of Chemistry for Energy Materials, Fudan University, Shanghai 200433, PR China
[b] Chinese Academy of Science, Institute of Physics, Laboratory of Advanced Materials & Electron Microscopy, Beijing 100190, PR China
[c] Department of Chemistry, Boston College, Chestnut Hill, MA 02467, USA
[d] Chinese Academy of Science, Ningbo Institute of Material Technology & Engineering, Ningbo 315201, PR China
[e] Department of Materials Science, Fudan University, Shanghai 200433, PR China
[f] Tianmu Lake Institute of Advanced Energy Storage Technologies Co. Ltd., Liyang, 213300, Jiangsu, China

ARTICLE INFO

Keywords:
Li metal batteries
Solid electrolyte interphase
Carbonate-based electrolyte
High-energy-density
Cryo-EM

ABSTRACT

Reducing the ratio of Negative/Positive ratio (N/P ratio) is critical to increase the energy density of Li metal batteries (LMBs). Typically, stable Li deposition with high Coulombic Efficiency (CE) can be easily achieved with ether-based electrolyte, but the low oxidation stability restrains its applications in batteries with high-voltage cathodes. Herein, we performed cryogenic electron microscopy (Cryo-EM), in-depth X-ray Photoelectron spectrum (XPS) and Atomic Force Microscopy (AFM) on the Solid Electrolyte Interphase (SEI) layer formed in carbonate-based electrolyte and ether-based electrolyte to probe the characteristics of good SEI layer and aimed to design good SEI layer in carbonate-based electrolyte by tuning the electrolyte composition. The results suggest that the organic composition in the SEI layer determine the CE of LMBs. Further theoretical calculation suggests the highly reactive nature of carbonate molecules with Li results in the organic-rich SEI layer with low elastic modulus. On the basis of these insights, we propose design methodology for an advanced SEI layer in carbonate electrolyte by tuning the electrolyte composition. The designed SEI exhibits multilayer structure with a dense inorganic inner layer. Consequently, a 4 V full cell was assembled and delivered a high energy density of 760 Wh/kg (calculated based on the weight of cathode and anode) with long cycle life of 200 cycles in carbonate electrolyte.

1. Introduction

With the energy density of current Li-ion batteries approaching their theoretical limit, there is urgent requirement for batteries with high energy density to extend the range of electrical vehicles. Li metal batteries (LMBs) are attractive because Li metal anode enables to increase the energy density by 40–50% than the conventional graphite-based lithium ion batteries [1–3]. However, the high theoretical energy density of LMBs could only be achieved when limited Li metal anode is coupled with high-energy cathode (e.g. NCM811) [4,5]. Unfortunately, LMBs with long cycle stability were usually obtained with over 10-fold excess of Li metal [6–12]. As a result, the energy density of LMB is compromised. Actually, many LMBs reported in the literatures [6–12] are less energy dense than Li-ion cells due to the substantial amount of Li excess in the anode. Hence, it is quite critical to limit the Li excess and reduce the negative/positive capacity ratio (N/P ratio) in the LMBs.

Nevertheless, it is a great challenge to limit the Li excess, since the Li deposition process is usually accompanied with large volume expansion and severe dendrites formation, leading to the continuous pulverization and formation of solid electrolyte interphase (SEI) accompanied with the formation of "dead lithium". This process inevitably consumes active Li metal, causing irreversible inventory Li loss [1].

To achieve the theoretically high energy density of LMBs, stable Li plating/stripping with a high coulombic efficiency (CE) is a necessary

* Corresponding authors.
** Corresponding author at: Chinese Academy of Science, Institute of Physics, Laboratory of Advanced Materials & Electron Microscopy, Beijing 100190, PR China.
E-mail addresses: shencai@nimte.ac.cn (C. Shen), lucas.bao@bc.edu (J.L. Bao), wxf@iphy.ac.cn (X. Wang), yyxia@fudan.edu.cn (Y. Xia).

https://doi.org/10.1016/j.nanoen.2021.105847
Received 18 November 2020; Received in revised form 20 December 2020; Accepted 30 January 2021
Available online 4 February 2021

prerequisite. Typically, high CE of Li plating/stripping can be easily achieved in the ether-based electrolyte with $LiNO_3$ additives, but the low anodic limit of ether-based electrolyte restricts their application in high-voltage LMBs [13–16]. Therefore, research attention is mainly focused on extending the anodic limits of ether-based electrolyte by applying high concentration electrolytes (HCEs) [17–19], localized high concentration electrolyte (LHCEs) [4,20–24], designing novel fluorinate solvents [25] or freezing the ether solvents in the pore of metal organic framework [26]. Among these strategies, HCEs and LHCEs are promising for the practical application of high-voltage LMBs. The HCE successfully reduces the free-solvent molecular, leading to the enhancement of the oxidation stability. When diluted with non-solvating fluorinated ether molecules, the drawback of high viscosity and high cost of Li salts have been addressed. Hence, the LHCE shows promising for LMBs under practical condition [4]. Besides, designing novel fluorinate solvent [25] that is stable towards both Li metal anode and high-voltage cathode is also highly desirable for the practical LMBs. Nevertheless, most newly designed fluorinated solvents are not commercially available. Consequently, strenuous organic total synthesis and purification process are inevitable.

On the other hand, carbonate-based electrolyte, which exhibits high anodic stability over 4.0 V, fails in the LMBs. Previous reports showed that the CE for Li deposition in the 1 M $LiPF_6$ EC/DEC is usually below 80% [27–29], indicating the severe consumption of active Li metal during cycles in the carbonate electrolyte. As a result, the Li metal full cell decays rapidly under low N/P ratio condition in the carbonate electrolyte. To date, it is still challenging to achieve long-term cycle of LMBs in carbonate-based electrolyte with limited Li in the anode. Even worse, the primary cause for the poor CE of Li anode in carbonate-based electrolytes is also elusive. Only recently, Wang et al. [19] report a super concentrated carbonate-based electrolyte (10 M LiFSI in DMC) for LMBs, but the high viscosity and high cost of Li salt hinder its practical applications. Recently, FEC solvent has employed for Li metal batteries with improved performance because FEC solvent can form better SEI layers compared with EC [30–32], but the characteristics(e.g. composition, structure and mechanic property) of better SEI layers is still unknown. Although some predesigned polymer or inorganic-based SEI layers such as LiF rich SEI layer on shows excellent performance for Li deposition in the carbonate electrolyte [11,33], the designed principle for advanced SEI layer formed in-situ in carbonate solvents is still deficient.

Herein, we performed Cryo-EM, AFM and In-depth XPS on the SEI layers with different CE to probe the characteristics (i.e. composition, structure, mechanic property) of good SEI layers and aimed to design good SEI layer in the carbonate electrolyte, since carbonate-based electrolyte is more suitable for high-voltage cathode. The results suggest that the SEI layer becomes soft when the organic compositions in the SEI layer mixes with the inorganic compounds, which is prone to be pierced by Li dendrites, leading to the low CE of Li plating/stripping in the carbonate electrolyte. In addition, Density Function Theory (DFT) was also employed to investigate the reactivity of different solvents with Li metal. The result suggests that the ROCOOR groups in carbonate molecules are more likely to react with Li metal compared with ether molecules, resulting in the surplus organic composition in the SEI layer. On this basis, we propose the design methodology for advanced SEI in carbonate electrolyte by optimizing the electrolyte composition. The designed SEI layer exhibits multilayer structure with a dense inorganic layer and ultrathin organic outer layer. As a result, a high CE of Li plaiting/stripping is achieved with designed SEI in the carbonate electrolyte. A 4 V full cell was assembled and delivered a high energy density of 760 Wh/kg (calculated based on the weight of cathode and anode materials) with long cycle life of 200 cycles in the carbonate electrolyte. The achieved performances are among the best ever reported under the same condition (see Table S1 for comparison).

2. Experimental section

2.1. Materials

Fluoroethylene carbonate (FEC), 1,1,2,2-Tetrafluoroethyl 2,2,2-trifluoroethyl ether (HFE), lithium bis-trifluoromethanesulfonimide (LiTFSI), 1,3-dioxolane (DOL), Ethylene glycol dimethyl ether (DME), Ethylene carbonate (EC) Diethyl carbonate (DEC), $LiPF_6$ and $LiNO_3$ were purchased from Nanjing Mojiesi Energy Tech. Lithium bis-fluorosulfonimide (LiFSI) was purchased from General Motors Limits. Commercialized NCM811 powder was purchased from BASF. $LiPO_2F_2$ was purchased from SuZhou Fluolyte Co. All the reagents were used without any further purification.

2.2. Electrolyte and electrode preparation

six kinds of electrolytes were prepared by dissolving different amount of Li into the solvent in the glove box filled with Ar. The electrolyte compositions is (1): 1 M $LiPF_6$ EC/DEC (1:1); (2) 1 M LiFSI EC/DEC (3) 1 M LiTFSI DOL/DME (1:1); (4) 1 M LiTFSI DOL/DME (1:1) 2 wt % $LiNO_3$; (5) 6 M LiFSI EC/DEC (1:1); (6) 2.2 M LiTFSI, 0.2 M $LiPO_2F_2$ FEC:HFE (2:1). To prepare the electrode, commercialized NCM811 powder was mixed with Super P and PVDF in a ratio of 9:0.5:0.5 and then dispersed into N-Methyl pyrrolidone (NMP) solvent. The mixture was then slurried on a carbon coated Al foil. Subsequently, the electrode was dried under vacuum for 24 h at 80 °C to remove the residual NMP solvent. The average active material loading is about 15 mg cm^{-2}. The Li on Cu foils were prepared by electro-depositing 1.5 mAh cm^{-2} (N/P = 0.5) or 3 mAh cm^{-2} (N/P = 1) on the Cu foils at the current density of 0.5 mA cm^{-2} in the corresponding electrolyte. Graphite anode was also prepared. Graphite was mixed with Super P and PVDF in a ratio of 8:1:1 in the NMP solvent. The mixture was then slurried on the Cu foil. The average loading of graphite is 1 mg cm^{-2}.

2.3. Electrochemical test

To evaluate the electrochemical performance of the solid electrolyte interphase formed in different electrolyte, Li||Cu, Li||NCM811 and G(1 mg cm^{-2})||NCM811(15 mg cm^{-2}) were assembled in CR2032 coin cells. The Li||Cu half-cell was prepared by separating Li chip (250 μm) and Cu foil with a $LiNO_3$ functionalized glass fiber separator dipping with 100 μl electrolyte. To prepare the $LiNO_3$ functionalized glass fiber, 1 g $LiNO_3$ was dissolved in the 10 ml DME solvent, and then glass fiber was immersed in the solution for 2 h. Finally, the glass fiber was dried under vacuum to obtain the $LiNO_3$ functionalized glass fiber separator. Prior to Li deposition, the Li||Cu half-cell was cycled at 0.05 mA cm^{-2} between 0 V and 1 V for 10 cycles. For Li||NCM811 cell assembly, 1.5 mAh cm^{-2} or 3 mAh cm^{-2} Li was deposited on the Cu foil in the 2.2 M LiTFSI 0.2 M $LiPO_2F_2$ FEC: HFE (2:1) electrolyte and then the Li@Cu electrode was extracted from the half-cells, washed with DME solvent for several times and then dried under vacuum for 12 h. The Li||NCM811 full cell was assembled by separating the Li@Cu electrode and NCM811 cathode (15 mg cm^{-2}) with glass fiber separator dipping with 100ul electrolyte. The graphite (1 mg cm^{-2}) || NCM811 (15 mg cm^{-2}) full cell was also prepared by the same method. For the charge/ discharge test, the full cells were charged at 0.1 C and discharged at 0.2 C for the initial cycle, and then were full cells were charged at 0.2 C and discharged at 0.5 C for the following cycles.

2.4. Characterization

SEM images were taken on the FE-SEM S-4800. In-depth X-ray photoelectron spectroscopy (XPS) was carried out on aXSAM800 Ultra spectrometer. The electrodes for XPS test were transferred into the XPS chamber with an air-free holder filled with Argon. Atomic Force Microscopy (AFM) (Bruker Icon) experiments were conducted in a

glovebox (MBRAUN, $H_2O \leq 0.1$ ppm, $O_2 \leq 0.1$ ppm) at room temperature. Prior to AFM test, the Li||Cu half cells were assembled in a glove box with different electrolytes. Then, 1 mAh cm^{-2} of Li metal was deposited on the Cu foil in the different electrolytes at 0.5 mA cm^{-2}. The Li@Cu foils were then extracted from the Li||Cu half-cell and washed with DME solvent to remove the residual Li salts. The Li metal for the Transmission Electron Microscopy (TEM) was directly deposited on a lacey carbon grid in a coin cell for 20 min at 0.5 mA cm^{-2}. The grid was taken out and slightly rinsed with DMC to remove trace Li salt. Then it was transferred into the cryo-TEM holder in an Ar-filled glove box. Using a sealed container, the cryo-TEM holder was quickly inserted into JEOL JEM-ARM200F, and then, liquid nitrogen was poured into the cryo-TEM holder until the sample temperature dropped below − 180 °C. All cryo-TEM characterizations were carried out using an aberration-corrected microscope (JEOL JEM-ARM200F) under cryogenic temperatures (− 180 °C) at 200 kV. Lattice spacings of Li metal and its salts were analyzed using Digital Micrograph (Gatan) software.

2.5. Computational details

Computational details are given in the Supporting Information.

3. Result and discussion

3.1. Characterization of SEI layers formed in different electrolytes

Unlike the graphite anode in Li-ion batteries, Li metal anode undergoes large volume change during repeated cycles, accompanying with severe dendrite growth. Conventional SEI layers formed in carbonate-based electrolyte are not stable towards Li metal anode. As a result, LMBs are usually cycled in ether-based electrolyte with $LiNO_3$ additives [13–16].

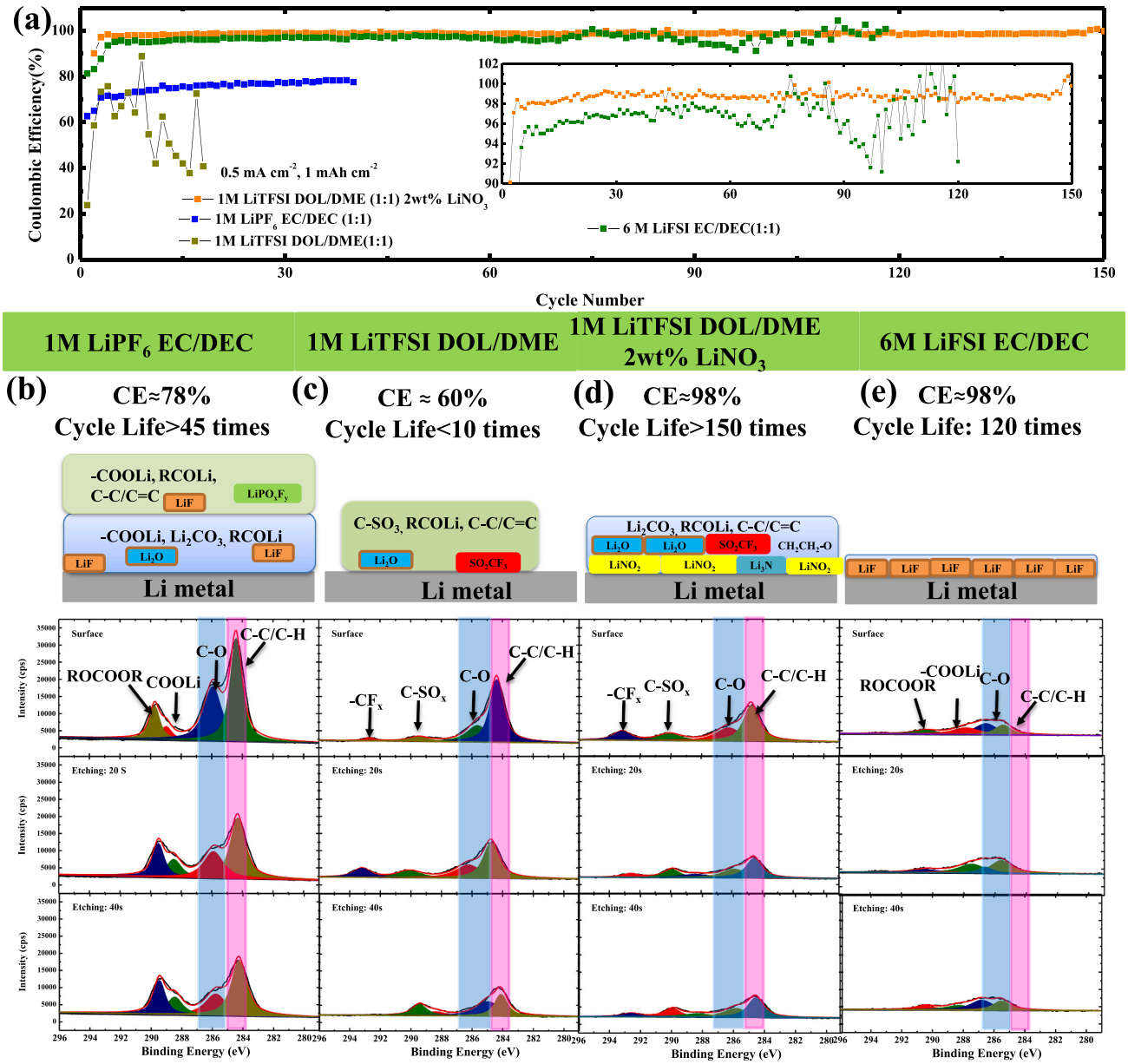

Fig. 1. Characterization of composition of the SEI layers in different electrolyte: a) CE of Li plating/stripping in different electrolyte; b) *C 1s* in-depth XPS spectrum of Li metal surface in 1 M $LiPF_6$ EC/DEC; c) *C 1s* in-depth XPS spectrum of Li metal surface in 1 M LiTFSI DOL/DME; d) *C 1s* in-depth XPS spectrum of Li metal surface in 1 M LiTFSI DOL/DME 2 wt% $LiNO_3$; e) *C 1s* in-depth XPS spectrum of Li metal surface in 6 M LiFSI EC/DEC.

To probe the difference of the SEI layers formed in ether-based electrolyte and carbonate-based electrolyte, a series of electrolytes were prepared to investigate the CE of Li plating/stripping on Cu foils. As shown in Fig. 1**a**, the CE of Li deposition in 1 M $LiPF_6$ EC/DEC is only 62.65% at the initial cycle, which was then increased and stabilized at 77% for over 40 cycles. In 1 M LiFSI EC/DEC, the CE of Li deposition is similar with the one in 1 M $LiPF_6$ EC/DEC (Fig. S1). The result suggests that the kind of salts, which contributes to the inorganic species in the SEI layer, has little influence on the CE of Li deposition in the carbonate-based electrolyte. When the salt concentration increases to 6 M, the initial CE of Li plating/stripping in 6 M LiFSI EC/DEC increases to 81% and then stabilizes at 96% after 10 cycles. The CE of Li deposition maintains 96% for 90 cycles in the 6 M LiFSI EC/DEC, and then begins to fluctuate. While in ether-based electrolyte, the initial CE of Li plating/stripping in 1 M LiTFSI DOL/DME is 22% and then fluctuate violently in the absence of $LiNO_3$ additives, indicating the instability of Li deposition. However, after adding 2 wt% $LiNO_3$ additives, the CE of Li plating/stripping increases to 90% at the initial cycle and then stabilized at 98.5% for over 150 cycles.

To gain insight into the cause for the CE difference in the electrolyte, a series of characterizations including In-depth XPS, scanning electron microscopy (SEM), Cryo-EM, and AFM were performed on the Li metal to compare the composition, structure and mechanic property of these SEI layers. Fig. 1**b**–1**d** exhibits the *C 1s* in-depth *XPS* of Li metal in different electrolyte. Compared with ether-based electrolyte, organic species especially –COOLi and ROCOOR species are much more prevalent in the SEI layer with $LiPF_6$ EC/DEC (Fig. 1**b**). After Ar^+ spur, the peak intensity corresponding to –COOLi and ROCOOR groups does not change, while the peak intensity of C–C/C=C and C–O decrease after Ar^+ spur. This result indicates –COOLi and ROCOOR species are prevalent in all layer of SEI, while the C–C/C–O species are mainly located on the surface of SEI layer. On the other hand, the peak intensity of LiF increases after Ar^+ spurring in the F 1s spectrum (Fig. S2). The result indicates that the SEI layer is consisted of mixed organic-inorganic composition, where LiF and Li_2O permeated in the ROCOOR and –COOLi layer, while C–C/C=C or C–O species are mainly located on the surface. When the salt concentration increases to 6 M, the peak intensity and peak areas of corresponding to C–C/C=C, C–O, –COOLi and

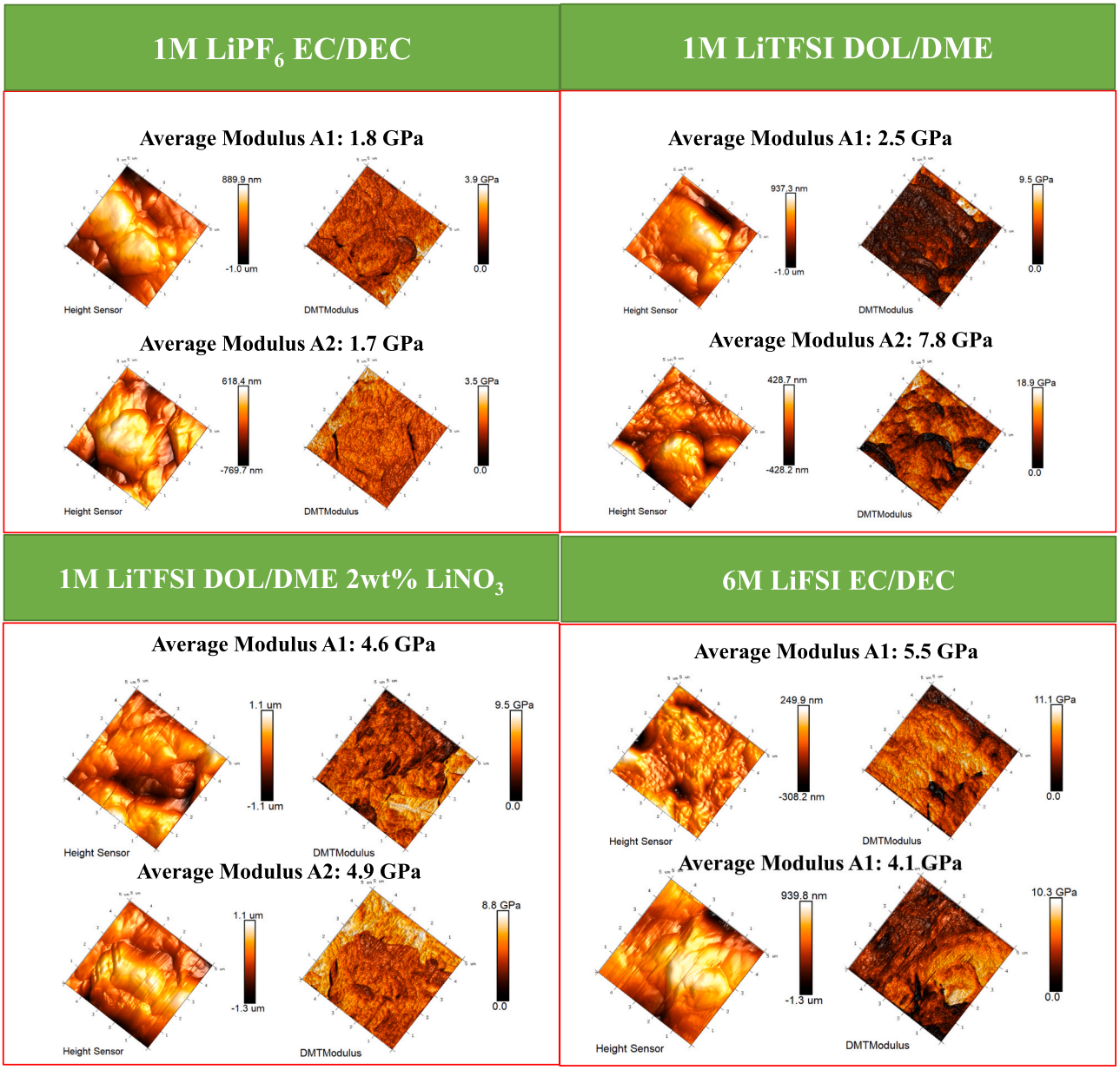

Fig. 2. Mechanic property of SEI layer formed in different electrolyte measured by Atomic Force Microscopy.

ROCOOR reduces, indicating the decrease of organic species in the SEI layer.

On the other hands, in the ether-based electrolyte, compared with carbonate electrolyte, the organic species corresponding to –COOLi and ROCOOR are not observed in the C 1s spectrum. In 1 M LiTFSI DOL/DME without $LiNO_3$ additives, the SEI layers derived from solvents and salts are not able to cover the surface of Li metal, leading to the poor performance of LMBs (also See the AFM result in Fig. 2). When $LiNO_3$ additives was added into the electrolyte, $LiNO_3$ can be decomposed to form ultrathin and dense $Li_xN_yO_z$ and Li_3N passivation layer (see *N 1s* Spectrum in Fig. S3). Hence, both cycling stability and CE of Li deposition is largely improved. These results suggest that surplus organic species especially ROCOOR or –COOLi in the SEI layer are the main cause for the low CE of Li deposition in the carbonate electrolyte. The *Li 1s* XPS spectrum is also given in Fig. S4, where the inorganic Li compounds are more prevalent in the electrolyte with high CE.

To further gain insight the cause of difference in CE in the electrolyte, AFM combined with SEM were carried out to gain insight into the mechanic property and the morphology of Li metal in different electrolytes. Fig. 2 shows the elastic modulus of SEI layers formed in different electrolyte. Two regions on the Li metal surface were measured by AFM. It can be observed that the elastic modulus of SEI layers formed in the 1 M $LiPF_6$ EC/DEC is 1.7 GPa and 1.9 GPa respectively in two regions. When the salt concentration increases to 6 M LiFSI in EC/DEC, the elastic modulus also increases to 4.1 GPa and 5.5 GPa respectively. On the other hand, in the ether-based electrolyte, the elastic modulus is 2.5 GPa and 7.8 GPa respectively in the absence of $LiNO_3$ additives. The large discrepancy of the elastic modulus in the two regions indicates the non-uniform distribution of the SEI layer in 1 M LiTFSI DOL/DME. It should be also noted that the elastic modulus of Li metal is 7.8 GPa [34], indicating that some regions of Li metal in 1 M LiTFSI DOL/DME does not cover with SEI layer, which is responsible for the poor performance of Li deposition in 1 M LiTFSI DOL/DME electrolyte. When 2 wt% $LiNO_3$ additives was added into the 1 M LiTFSI DOL/DME electrolyte, the elastic modulus of the SEI layer increased to 4.6 GPa and 4.9 GPa respectively. In conclusion, the SEI layers with high CE exhibit higher elastic modulus above 4.0 GPa, indicating the stability of SEI layer. Our result is also consistent with previous simulation [35], which shows that the elastic modulus should be above 3.0 GPa to stabilize the SEI layers. The results of AFM combined with in-depth XPS suggest that SEI layers with surplus organic composition become soft, which are more vulnerable to be pierced by the Li dendrites, leading to the low CE in the electrolyte.

We also performed the SEM to characterize the morphology of Li metal in different electrolyte. As shown in Figs. S5–S8, a loose Li deposition with obviously porous structure is observed in the SEM images with 1 M $LiPF_6$ EC/DEC (Fig. S5). When the salt concentration increases to 6 M, the deposited Li metal in 6 M LiFSI EC/DEC becomes much denser, but some cracks of Li metal can be also observed (Fig. S8). This indicates that the SEI formed in 6 M LiFSI EC/DEC is lack of

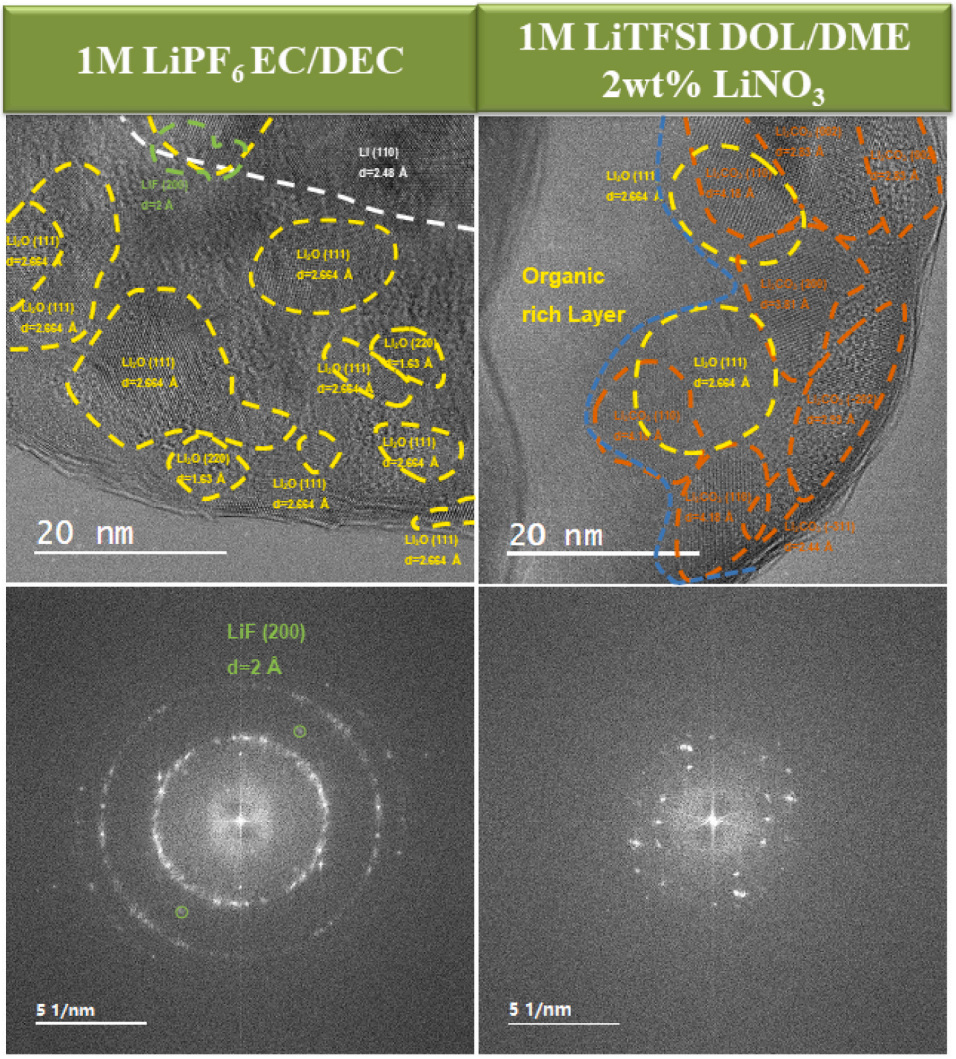

Fig. 3. Cryogenic TEM images and FFT images of SEI layer formed in $LiPF_6$ EC/DEC and LiTFSI DOL/DME 2 wt% $LiNO_3$.

elasticity. In 1 M LiTFSI DOL/DME electrolyte, obvious dendrites with loose Li deposition were observed in the absence of $LiNO_3$ (Fig. S6). However, after adding $LiNO_3$ into the electrolyte, a dense and smooth Li deposition without any dendrites and cracks was observed in the ether-based electrolyte with 2 wt% $LiNO_3$ (Fig. S7).

The Cryo-TEM was also carried out to further gain insight into the structure of SEI layers formed in different electrolyte. SEI layers formed in two kind of electrolytes containing 1 M $LiPF_6$ EC/DEC and 1 M LiTFSI DOL/DME 2 wt% $LiNO_3$ were selected for Cryo-TEM comparison. To prepare the samples for Cryo-EM test, Li metal was deposited on the micro-grid with at 0.5 mA cm^{-2} for 20 min in the electrolytes for a convenient observation by TEM. As shown in Fig. 3, the SEI layers formed in the $LiPF_6$ EC/DEC electrolyte shows a mosaic structure. It can be observed that the inorganic species such as LiF, Li_2O and the organic species such as –COOLi, ROCOOR are precipitated and randomly embedded in the SEI layer, forming a mosaic microphase. In addition, some characteristic bright diffraction spots corresponding to LiF (200) plane were also captured in the fast Fourier transformed (FFT) image. The result suggests that a low CE of Li deposition can be still obtained even with LiF species in the SEI layer. For comparison, a multilayer structure with an organic rich inner phase and inorganic rich outer layers was observed in the 1 M LiTFSI DOL/DME 2 wt% $LiNO_3$ electrolytes. In addition, the outer inorganic rich layer is comprised of Li_2CO_3 and Li_2O species, and none LiF is found in the SEI layer. Although previous report [36] suggests that fluorinated species are important to stabilize the SEI layer for LMBs, we find the content and distribution of organic species in the SEI layer are more important to determine the CE of Li plating/stripping.

We also investigate the evolution of electrochemical impedance of Li||Li symmetric cells using in 1 M $LiPF_6$ EC/DEC and 1 M LiTFSI DOL/DME 2 wt% $LiNO_3$. To investigate the evolution of impedance over cycles, 3 mAh cm^{-2} Li was deposited on the Cu foil at 0.5 mA cm^{-2} and then Li||Li@Cu symmetric cell was cycled at 0.5 mA cm^{-2} with a fixed capacity of 0.5 mAh cm^{-2}. The Li||Li@Cu symmetric cell died after 10 h in 1 M $LiPF_6$ EC/DEC electrolyte, while the Li||Li@Cu symmetric cell runs over 40 h. As shown in Fig. S9, the Li||Li@Cu symmetric cell shows initial impedance of 31.4 Ω, which then increases to 1140Ωafter 10 h in 1 M $LiPF_6$ EC/DEC. For comparison, the impedance decreases from 51.9 Ω to 4.7 Ω after 40 h in 1 M LiTFSI DOL/DME 2 wt% $LiNO_3$. This result suggest the SEI layer formed in the LiTFSI DOL/DME 2 wt%$LiNO_3$ is more stable compared with the one formed in 1 M $LiPF_6$ EC/DEC.

Above all, by combining the result of in-depth XPS, AFM, SEM and Cryo-EM, we conclude that the distribution and content of organic species rather than LiF play decisive role to determine the CE of Li deposition. Therefore, a desired SEI layer should exhibit a moderate elastic modulus over 3.0 GPa [35] with a multilayer structure, which is comprised of a dense inorganic layer to increase the mechanic strength of SEI layer and an organic rich layer to buffer the volume expansion.

3.2. *Design strategy of advanced SEI layers in carbonate-based electrolytes*

As discussed above, the content and distribution of organic compositions plays the decisive role to determine the CE of Li deposition. Since the organic compositions in the SEI layer come from the decomposition of organic solvent, we investigated the reactivity of several organic solvents on Li metal by Density Functional Theory calculations.

The reduction of organic solvents and the formation of SEI layer on the Li metal surface involve a series of complex processes including adsorption of solvent molecules on the Li metal surface, electron

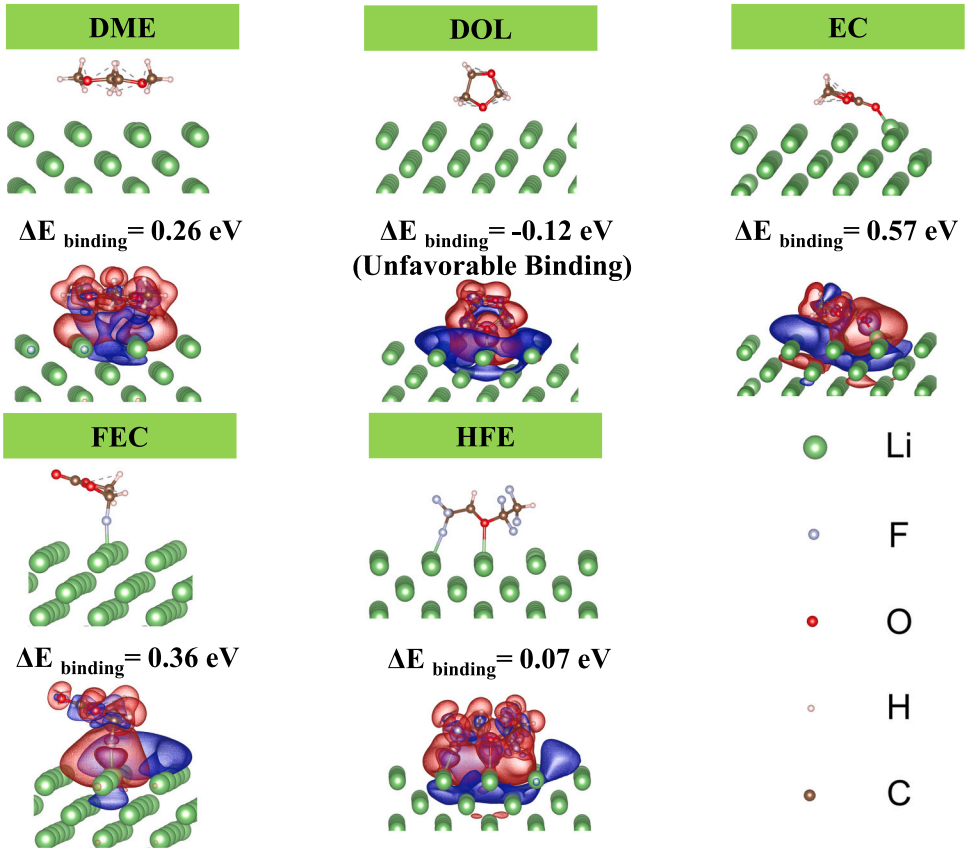

Fig. 4. Theoretical calculation of the binding energy and charge density of different solvents on Li metal (The calculated differential charge density is shown as the isosurface plot, with an isosurface value of 3.6×10^{-8} $e/Å^3$. region (an increase in charge density) is in blue, and region (a decrease in charge density) is in vermilion.). (For interpretation of the references to colour in this figure legend, the reader is referred to the web version of this article.)

transferring process and the reduction of solvent molecules. Among these processes, the initial adsorption of solvent molecules on the Li metal is the rate-determining step [37–39], which determines the following decomposition product of SEI layers. Therefore, we investigate the binding geometry, binding energy and electronic charge density of several solvent molecules on the Li metal. As shown in Fig. 4, compared with carbonate solvent molecules (EC and FEC), the binding energy of ether-based solvent molecules are much weaker, indicating that the reactivity of ether-based solvent molecules on Li metal is much weaker. Especially, for DOL molecules, the binding energy of DOL on Li metal is − 0.07 eV, indicating that the DOL molecules are not likely to react with the Li metal. Nevertheless, the O atoms in the carboxyl group (–C=O) in the EC molecules becomes the reactive site for Li metals, which is vulnerable to attack the Li metal. The primary chemical bonds formed between EC and Li is Li–O=C bond. However, when the H atom in EC is substituted by electronegative F atom to form FEC solvent, the electronegative F atom becomes the reactive site for Li and the primary chemical binding of FEC on the Li metal become the Li–F bond. Above all, in the carbonate-based electrolyte, the lithium salts must compete with the carbonate solvent to react with Li metal. Hence, a mosaic SEI layer with mixed matrix of organic species and inorganic compounds is likely to be formed. Nevertheless, in the ether-based electrolyte, the decomposition of Li salts becomes the main source of inner SEI layers, while the ether solvent polymerizes on the surface of the inner inorganic SEI layers to soft outer layer to accommodate the volume expansion during Li deposition.

We also calculated the electronic charge density of different solvents on the surface of Li metal. It is observed that the electronic charge density of all the solvents increases on the interface of Li metal, indicating the favorable formation of chemical bond between solvent and Li metal. However, the decrease of electronic charge density is between F–C for FEC and C=O for EC, indicating LiF is more likely to form in the FEC electrolyte while organic species such as –COOLi or ROCOOR is vulnerable to form in the EC electrolyte. As a result, it is expected that fewer organic derived products are formed in the FEC solvent compared with EC solvent [37,38].

Hence, to design the multilayer SEI layers on the Li metal surface in the carbonate electrolyte, FEC is selected as the solvent to construct the inner inorganic rich SEI layer since more inorganic compositions are formed during the decomposition of FEC [37,38]. In order to further increase the content of inorganic composition in the inner SEI layer, an intermediate salt concentration of 2.2 M LiTFSI and 0.2 M $LiPO_2F_2$ is also applied. The $LiPO_2F_2$ salt not only increases the inorganic content in the SEI layer, but also prevents the corrosion of Al foil. At the same time,

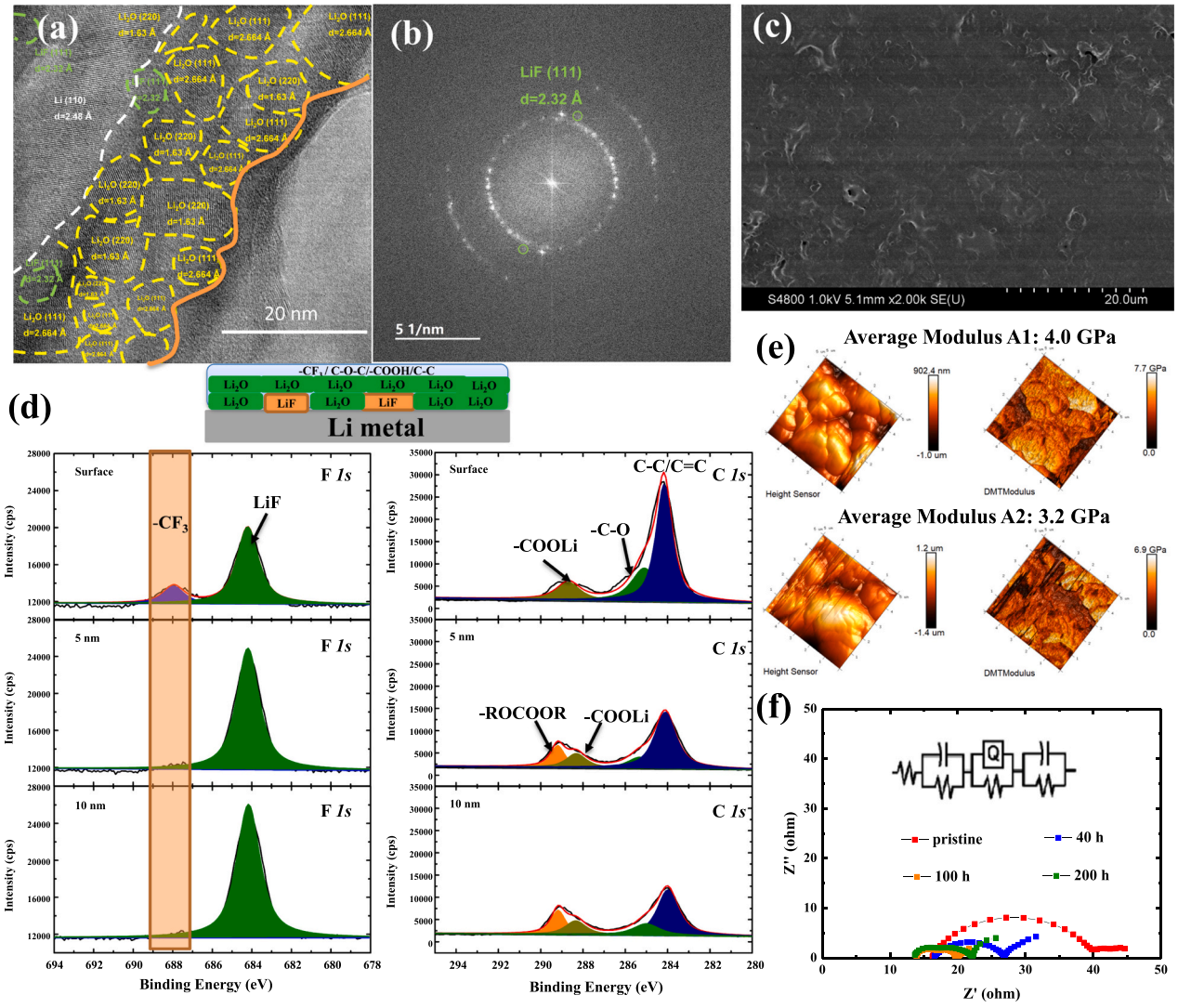

Fig. 5. Characterization of the designed SEI layer: a) Cryo-TEM image of the designed SEI layer; b) FFT image of the designed SEI layer; c) SEM image of Li metal with the designed SEI layer; d) In-depth XPS of the designed SEI layer; e) mechanic property of the designed SEI layer; f) EIS spectrum of designed SEI layer over cycles.

the $LiPO_2F_2$ additives can also form $LiPO_xF_y$ CEI layer on the NCM811 cathode, and thus stabilize the structure of NCM811 cathode [39]. Besides, an organic-rich layer is also essential to buffer the volume expansion of Li metal. HFE, which has poor solvability of Li ions and weak reactivity with Li metal, is selected to construct the outer organic rich layers. Hence, it is expected that a multilayer SEI with dense LiF, Li_2O rich inner layer and organic rich outer layer is formed in the 2.2 M LiTFSI, 0.2 M $LiPO_2F_2$ FEC/HFE (2:1) electrolyte.

To characterize the SEI layer formed in 2.2 M LiTFSI, 0.2 M $LiPO_2F_2$ FEC/HFE (2:1) electrolyte, Cryo-TEM combined with in-depth XPS, AFM and SEM were carried out. As shown in Fig. 5**a**, the SEI layer in 2.2 M LiTFSI, 0.2 M $LiPO_2F_2$ FEC/HFE (2:1) electrolyte exhibits a multilayer structure, which is comprised of a Li_2O rich inner layer and an organic rich outer layer. Notably, even in this all fluorinated electrolyte, LiF species are rarely observed in the compact SEI layers, which is also confirmed by FFT images. As shown in Fig. 5**b**, the diffraction spot corresponding to LiF (1,1,1) crystal plane is dim, indicating that LiF is rarely found in the SEI layer even in this all fluorinated electrolyte Further evidence of EDS mapping also confirm that LiF is absent in the compact SEI layer. As shown in Fig. S10, most of the LiF species were agglomerated as nano-balls rather than dispersed in the compact SEI layers, while the compact SEI layer is comprised of Li_2O species and N containing species. Our finding is also consistent with previous report that LiF is almost absent within the compact SEI film [40].

We also perform the SEM to characterize the morphology of Li metal in the electrolyte. As shown in Figs. 5**c** and S11, a smooth surface of Li metal without any crack and dendrite is observed with designed SEI layer. The in-depth XPS also shows that the surface of Li metal is consisted of organic compounds including C-C/C-O and -CF_3 species, while LiF become the dominant species after Ar^+ etching (Fig. 5**d**). The *Li 1s* XPS spectrum also confirms that Li_2O and LiF is the dominant species (Fig. S10). AFM was also carried out on the designed SEI layer to probe the mechanic property of the designed SEI layer. As shown in Fig. 5**e**, the two regions on the Li metal surface with the designed SEI layer exhibits an elastic modulus of 4.0 GPa and 3.2 GPa. The elastic modulus of SEI layer is above 3.0 GPa, which is strong enough to stabilize the SEI layer [35].

The electrochemical impedance spectrum (EIS) was also carried out to study the interfacial impedance of the designed SEI layer during cycles. To evaluate the interfacial impedance of SEI layer during cycles, Li||Cu half-cell was assembled. 3 mAh cm^{-2} Li was deposited onto the Cu foil, and then the cell was cycled at 0.5 mA cm^{-2} with a fixed capacity of 0.5 mAh cm^{-2}. The Li||Li@Cu half-cell gives a high interfacial impedance of 24 Ohm for the initial cycles, which is then reduced to 10 Ohm after 40 h. The interfacial impedance further decreases after 100 h. Even after 200 h, the interfacial impedance only slightly increases. The result suggests the stability of the designed SEI interface during cycles.

3.3. Electrochemical performance of the designed SEI layer

To demonstrate the electrochemical performance of the designed SEI layer, Li||Cu half-cell, Li||NCM811 full cell (N/P = 0.5 or 1) and Li-free LMBs were assembled with this optimized electrolyte.

As shown in Fig. S11, an initial CE of 92% is obtained in the optimized electrolyte, which then gradually increases to 98% and maintains at 98% for over 150 cycles at 0.5 mA cm^{-2} with a fixed capacity of 1 mAh cm^{-2} (Fig. S11a). When the current density increases to 1 mA cm^{-2} with a fixed capacity of 1 mA cm^{-2}, a high initial CE of 93% was obtained and the CE gradually increases to 98.5% for 200 cycles (Fig. S11b and S11c). When the current density further increases to 2 mA cm^{-2} with a fixed capacity of 1 mA cm^{-2}, a high average CE of 98.5% is also achieved in the optimized electrolyte (Fig. S11d and S11e). In addition, the polarization remains almost unchanged for 200 cycles at the current density of 2 mA cm^{-2}. To accurately determine the CE of LMBs, a method [41] proposed by Zhang et al. was employed. As shown in Fig. S12, an average CE of 99.0% is achieved with designed SEI layer in the carbonate-based electrolyte. Above all, the CE of Li deposition with advanced SEI layers in the optimized electrolyte can be even compared with the one formed in the ether-based electrolyte with $LiNO_3$ additives.

Fig. 6**a** and 6**b** shows the rate performance of NCM811 half-cell in the optimized electrolyte. The NCM811||Li metal half-cell shows a capacity of 203 mAh g^{-1} at 0.2 C, 184 mAh g^{-1} at 0.5 C and 165 mAh g^{-1} at 1 C. The specific capacity almost recovers to the initial capacity when the current density reduced to 0.2 C. To demonstrate the performance of the designed SEI layer in the optimized electrolyte under practical condition, NCM811||Li full cells were also prepared. The NCM811 cathode with high areal loading of 15 mg cm^{-2} was paired with limited Li@Cu foils (1.5 mAh cm^{-2} corresponding to N/P = 0.5 and 3 mAh cm^{-2} corresponding to N/P = 1) with 100 μl electrolyte. The cell was charged at 0.2C and discharged at 0.5 C. As shown in Fig. 6**c** and 6**e**, when NCM811 cathode was paired with 3 mAh cm^{-2} Li (N/P = 1), a specific discharge capacity of 184 mAh cm^{-2} is obtained after the initial activating cycle. Both the specific discharge capacity and the polarization of the batteries remain unchanged for 120 cycles. After 120 cycles, the specific capacity slightly reduces, but even after 200 cycles, a specific capacity of 160 mAh g^{-1} is also obtained, corresponding to capacity retention of 87%. When the amount of Li metal in the anode reduces to 1.5 mAh cm^{-2} (N/P = 0.5), a long cycle life of 100 times with a capacity retention of 86.5% is also achieved (Fig. 6**d** and 6**f**). The achieved performance is among the best in the carbonate-based electrolyte and can be even compared with those achieved in the localized high concentration ether-based electrolytes (see Table S1 for comparison.). For comparison, the NCM811 (15 mg cm_{-2})||Li (N/P = 0.5 or 1) full cells decays rapidly in the 1 M $LiPF_6$ EC/DEC electrolyte (Fig. S15).

To further demonstrate the performance of the designed SEI layer in the optimized electrolyte, the NCM811 cathode was also paired with Li-free anode. The Li-free batteries show the worst scenario of LMBs, since no extra Li source is provided. The NCM811 cathode (15 mg cm^{-2}) with a specific areal capacity of ~ 3 mAh cm^{-2} was directly paired with a thin layer of graphite (1 mg cm^{-2}) on Cu foil as Li metal host. Fig. S16a shows the CE of Li deposition on the graphite anode in the optimized electrolyte with a fixed capacity of 3 mAh cm^{-2} at the current density of 0.5 mA cm^{-2}. The cell shows an initial CE of 92%, which quickly increases to 99% within 10 cycles. Fig. S16b exhibits the corresponding voltage profiles of Li deposition in the graphite anode. It can be clearly seen in Fig. S16b that the capacity of Li ions intercalation into the graphite (1 mg cm^{-2}) is only about 0.35 mAh cm^{-2}, indicating that the graphite in the anode mainly act as a three-dimension (3D) conductive host for Li metal. The cycle stability and corresponding voltage profiles of NCM811 (15 mg cm^{-2}) ||Graphite (1 mg cm^{-2}) full cells were given in Fig. S16c and S16d. As shown in Fig. S16c, the Li metal full cell shows a specific discharge capacity of 182.4 mAh g^{-1} and a high CE of 94.8% after the initial activation cycles. Only after one cycle, the CE of the full cell reaches 99.3% and the CE maintains 99.3% for the following cycles. Even after 70 cycles, a specific capacity of 125.0 mAh g^{-1} is also achieved, corresponding to capacity retention of 70%. It should be noted that most of the anode-free LMBs were prepared after a pre-lithiation process, where dead lithium may present on the anode [5,42]. The morphology of Li deposition (3 mAh cm^{-2}) in the graphite host is also investigated by the SEM images. As shown in Fig. S17, a smooth surface without any dendrite was observed in the SEM images.

Above all, the designed SEI layer in the optimized electrolyte largely improves the electrochemical performance of LMBs with limited Li in the anode in the carbonate electrolyte.

4. Conclusion

In this work, by characterizing the SEI layers formed in the carbonate-based electrolyte and ether-based electrolyte with Cryo-EM, In-depth XPS, AFM and SEM, we identified that the content and

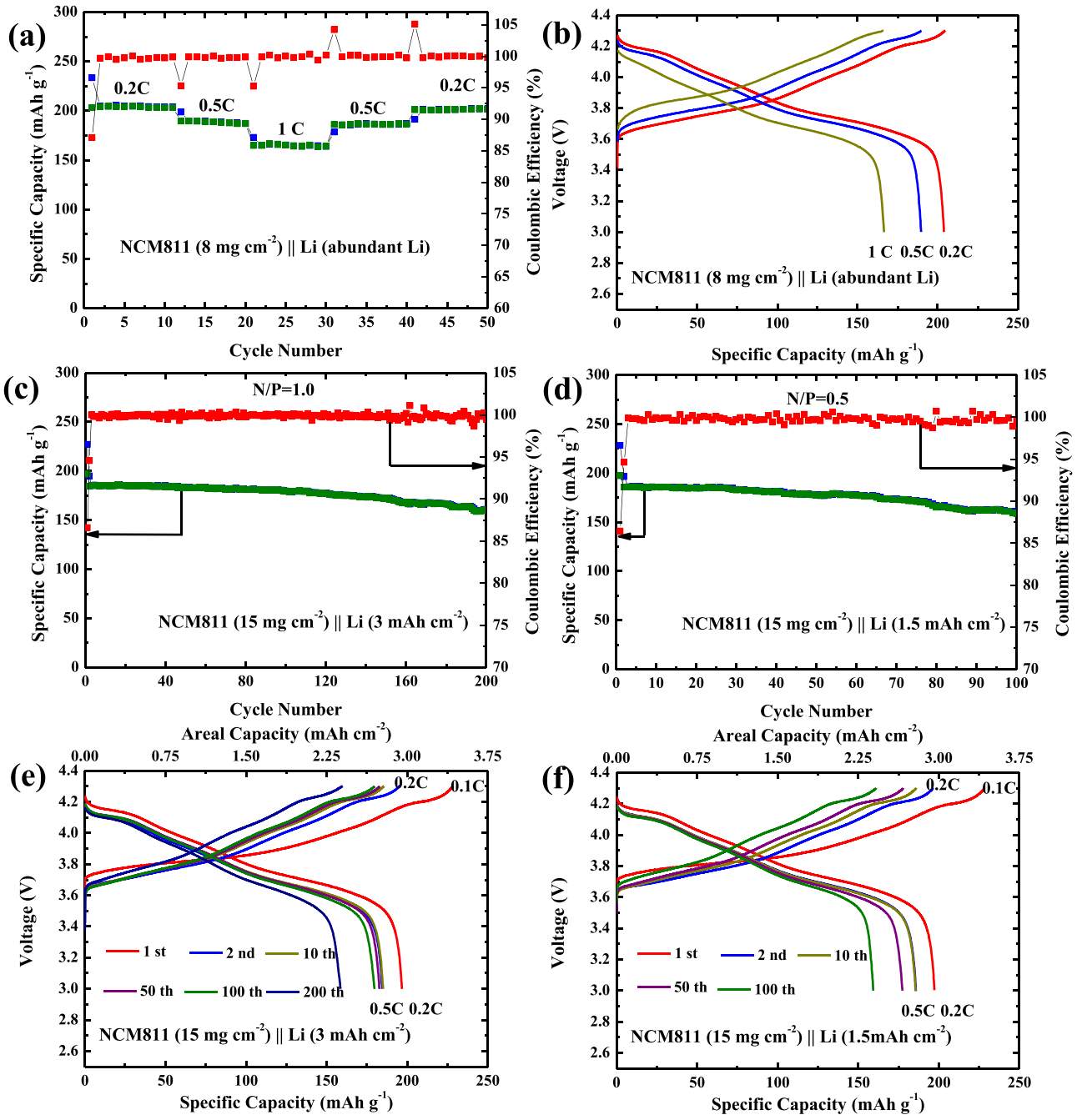

Fig. 6. Electrochemical performance of the NCM811||Li full cells with designed SEI layer: a) rate performance; b) the corresponding voltage profiles; c) Cycling performance of NCM811||Li full cell (N/P = 1); d) Cycling performance of NCM811||Li full cell (N/P = 0.5); e) Corresponding voltage profiles over cycles (N/P = 1); f) Corresponding voltage profiles over cycles (N/P = 0.5).

distribution of organic species in the SEI layers determine the CE of Li deposition in the electrolyte and then correlated the CE of Li deposition to the structure, mechanic property and composition of SEI layer. Further investigation by DFT calculation suggests that compared with ether molecular, carbonate molecular is more likely to react with Li metal and be decomposed on the surface to form organic-rich SEI layers. Based on the result, we present the methodology for designing advanced SEI layer by optimizing the electrolyte composition. The designed SEI layer exhibits high CE of Li plating/ striping in the carbonate electrolyte. As a result, the NCM811||Li (N/P = 1) can be cycle for 200 times with a capacity retention of 87%. Our work thus provides new insight for designing advanced SEI layer for practical LMBs.

CRediT authorship contribution statement

Shouyi Yuan conceived this idea and designed the experiment. Suting Weng and Xuefeng Wang carried out the Cryo–EM test and analyzed the data. Junwei Lucas Bao performed the theoretical calculation. Cai Shen carried out the Atomic Force Microscopy. Shouyi Yuan performed the materials synthesis, characterization, electrochemical measurement and data analysis. Shouyi Yuan, Suting Weng, Fei Wang and Junwei Lucas Bao co-wrote the manuscript. Yongyao Xia, Junwei Lucas Bao and Xuefeng Wang, Cai Shen direct the project. All the authors discussed the result and commented on the manuscript.

Declaration of Competing Interest

The authors declare that they have no known competing financial interests or personal relationships that could have appeared to influence the work reported in this paper.

Acknowledgement

We acknowledge the funding the National Natural Science Foundation of China (NSFC No. 21875045, 51372268 and 22005334), National Key Research and Development Program of China (2016YFB0901500, 2016YFB0100106 and 2018YFE0201702), the Shanghai Science and Technology Committee (19DZ2270100) Ningbo S&T Innovation 2025 Major Special Program (Grant No. 2018B10061) and start-up funding from Boston College.

Appendix A. Supporting information

Supplementary data associated with this article can be found in the online version at doi:10.1016/j.nanoen.2021.105847.

References

[1] W. Xu, J. Wang, F. Ding, X. Chen, E. Nasybulin, Y. Zhang, J.G. Zhang, Lithium metal anodes for rechargeable batteries, Energy Environ. Sci. 7 (2014) 513–537.
[2] J. Zheng, M.S. Kim, Z. Tu, S. Choudhury, T. Tang, L.A. Archer, Regulating electrodeposition morphology of lithium: towards commercially relevant secondary Li metal batteries, Chem. Soc. Rev. 49 (2020) 2701–2750.
[3] A.J. Louli, A. Eldesoky, R. Weber, M. Genovese, M. Coon, J. deGooyer, Z. Deng, R. T. White, J. Lee, T. Rodgers, R. Petibon, S. Hy, S.J.H. Cheng, J.R. Dahn, Diagnosing and correcting anode-free cell failure via electrolyte and morphological analysis, Nat. Energy 5 (2020) 693–702.
[4] X. Ren, L. Zou, X. Cao, M.H. Engelhard, W. Liu, S.D. Burton, H. Lee, C.J. Niu, B. E. Matthews, Z. Zhu, C. Wang, B.W. Arey, J. Xiao, J. Liu, J.G. Zhang, W. Xu, Enabling high-voltage lithium-metal batteries under practical conditions, Joule 3 (2019) 1662–1676.
[5] S. Yuan, J.L. Bao, N. Wang, X. Zhang, Y. Wang, D.G. Truhlar, D. G, Y. Xia, Salt-rich solid electrolyte interphase for safer high-energy-density Li metal batteries with limited Li excess, Chem. Commun. 56 (2020) 8257–8260.
[6] C.Y. Wang, Z.J. Zheng, Y.Q. Feng, H. Ye, F.F. Cao, Z.P. Guo, Topological design of ultrastrong MXene paper hosted Li enables ultrathin and fully flexible lithium metal batteries, Nano Energy 74 (2020), 104817.
[7] Q. Xu, J. Lin, C. Ye, X. Jin, D. Ye, Y. Lu, G. Zhou, Y. Qiu, W. Li, Air-stable and dendrite-free lithium metal anodes enabled by a hybrid interphase of C_{60} and Mg, Adv. Energy Mater. 10 (2020), 1903292.
[8] S. Yuan, J.L. Bao, J. Wei, Y. Xia, D.G. Truhlar, Y. Wang, A versatile single-ion electrolyte with a Grotthuss-like Li conduction mechanism for dendrite-free Li metal batteries, Energy Environ. Sci. 12 (2019) 2741–2750.
[9] X.Y. Yue, X.L. Li, W.W. Wang, D. Chen, Q.Q. Qiu, Q.C. Wang, X.J. Wu, Z.W. Fu, Z. Shadike, X.Q. Yang, Y.N. Zhou, Wettable carbon felt framework for high loading Li-metal composite anode, Nano Energy 60 (2019) 257–266.
[10] Y. Zhao, Q. Sun, X. Li, C. Wang, Y. Sun, K.R. Adair, R. Li, X. Sun, Carbon paper interlayers: a universal and effective approach for highly stable Li metal anodes, Nano Energy 43 (2018) 368–375.
[11] J. Bae, Y. Qian, Y. Li, X. Zhou, J.B. Goodenough, G.H. Yu, Polar polymer–solvent interaction derived favorable interphase for stable lithium metal batteries, Energy Environ. Sci. 12 (2019) 3319–3327.
[12] Y. Gao, M. Guo, K. Yuan, C. Shen, Z. Ren, K. Zhang, H. Zhao, F. Qiao, J. Gu, Y. Qi, K. Xie, B. Wei, Multifunctional silanization interface for high-energy and low-gassing lithium metal pouch cells, Adv. Energy Mater. 10 (2020), 1903362.
[13] S.S. Chi, Y. Liu, W.L. Song, L.Z. Fan, Q. Zhang, Prestoring lithium into stable 3D nickel foam host as dendrite-free lithium metal anode, Adv. Funct. Mater. 27 (2017), 1700348.
[14] L. Liu, Y.X. Yin, J.Y. Li, Y.G. Guo, L.J. Wan, Ladderlike carbon nanoarrays on 3D conducting skeletons enable uniform lithium nucleation for stable lithium metal anodes, Chem. Commun. 54 (2018) 5330–5333.
[15] S. Yuan, J.L. Bao, C. Li, Y. Xia, D.G. Truhlar, Y.G. Wang, Dual lithiophilic structure for uniform Li deposition, ACS Appl. Mater. Interfaces 11 (2019) 10616–10623.
[16] Q. Wang, K. Wu, H. Wang, W. Liu, Lithiophilic 3D SnS_2@carbon fiber cloth for stable Li metal anode, Acta Phys. Chim. Sin. 37 (2021), 2007092.
[17] J. Qian, W.A. Henderson, W. Xu, P. Bhattacharya, M. Engelhard, O. Borodin, J. G. Zhang, High rate and stable cycling of lithium metal anode, Nat. Commun. 6 (2015) 6362.
[18] J. Alvarado, M.A. Schroeder, T.P. Pollard, X.F. Wang, J.Z. Lee, M.H. Zhang, T. Wynn, M. Ding, O. Borodin, Y.S. Meng, K. Xu, Bisalt ether electrolytes: a pathway towards lithium metal batteries with Ni-rich cathodes, Energy Environ. Sci. 12 (2019) 780–794.
[19] X. Fan, L. Chen, X. Ji, T. Deng, S. Hou, J. Chen, J. Zheng, F. Wang, J.J. Jiang, K. Xu, C. Wang, Highly fluorinated interphases enable high-voltage Li-metal batteries, Chem 4 (2018) 174–185.
[20] Y. Yang, Y. Yin, D.M. Davies, M. Zhang, M. Mayer, Y.H. Zhang, E.S. Sablina, S. Wang, J.Z. Lee, O. Borodin, C.S. Rustomji, Y.S. Meng, Liquefied gas electrolytes for wide-temperature lithium metal batteries, Energy Environ. Sci. 13 (2020) 2209–2219.
[21] X. Ren, S. Chen, H. Lee, D. Mei, M.H. Engelhard, S.D. Burton, W. Zhao, J. Zheng, Q. Li, M.S. Ding, M. Schroeder, J. Alvarado, K. Xu, Y.S. Meng, J. Liu, J.G. Zhang, J. G, W. Xu, Localized high-concentration sulfone electrolytes for high-efficiency lithium-metal batteries, Chem 4 (2018) 1877–1892.
[22] S. Chen, J. Zheng, D. Mei, K.S. Han, M.H. Engelhard, W. Zhao, W. Xu, J. Liu, J. G. Zhang, High-voltage lithium-metal batteries enabled by localized high-concentration electrolytes, Adv. Mater. 30 (2018), 1706102.
[23] X. Fan, L. Chen, O. Borodin, X. Ji, J. Chen, S. Hou, T. Deng, J. Zheng, C. Yang, S. C. Liou, K. Amine, K. Xu, C.S. Wang, Non-flammable electrolyte enables Li-metal batteries with aggressive cathode chemistries, Nat. Nanotechnol. 13 (2018) 715–722.
[24] X. Wang, G. Pawar, Y. Li, X. Ren, M. Zhang, B. Lu, A. Banerjee, P. Liu, E.J. Dufek, J. G. Zhang, J. Xiao, J. Liu, Y.S. Meng, B. Liaw, Glassy Li metal anode for high-performance rechargeable Li batteries, Nat. Mater. 19 (2020) 1339–1345.
[25] Z. Yu, H. Wang, X. Kong, W. Huang, Y. Tsao, D.G. Mackanic, K. Wang, X. Wang, W. Huang, S. Choudhury, Y. Zheng, C.V. Amanchukwu, S.T. Hung, Y.T. Ma, E. G. Lomeli, J. Qin, Y. Cui, Z. Bao, Molecular design for electrolyte solvents enabling energy-dense and long-cycling lithium metal batteries, Nat. Energy 5 (2020) 526–533.
[26] Z. Chang, Y. Qiao, H. Deng, H. Yang, P. He, H. Zhou, A liquid electrolyte with de-solvated lithium ions for lithium-metal battery, Joule 4 (2020) 1776–1789.
[27] W. Zhang, Q. Wu, J. Huang, L. Fan, Z. Shen, Y. He, Q. Feng, G. Zhu, Y. Lu, Colossal granular lithium deposits enabled by the grain-coarsening effect for high-efficiency lithium metal full batteries, Adv. Mater. 32 (2020), 2001740.
[28] X.Q. Zhang, T. Li, B.Q. Li, R. Zhang, P. Shi, C. Yan, J.Q. Huang, Q. Zhang, A sustainable solid electrolyte interphase for high-energy-density lithium metal batteries under practical conditions, Angew. Chem. Int. Ed. 59 (2020) 3252–3257.
[29] J.Y. Hwang, S.J. Park, C.S. Yoon, Y.K. Sun, Customizing a Li–metal battery that survives practical operating conditions for electric vehicle applications, Energy Environ. Sci. 12 (2019) 2174–2184.
[30] Z. Yu, J. Zhang, C. Wang, R. Hu, X. Du, B. Tang, H. Qu, H. Wu, X. Liu, X. Zhou, X. Yang, G. Cui, Flame-retardant concentrated electrolyte enabling a LiF-rich solid electrolyte interface to improve cycle performance of wide-temperature lithium–sulfur batteries, J. Energy Chem. 51 (2020) 154–160.
[31] X. Zhang, X. Chen, X.B. Cheng, B.Q. Li, X. Shen, C. Yan, J. Huang, Q. Zhang, Highly stable lithium metal batteries enabled by regulating the solvation of lithium ions in nonaqueous electrolytes, Angew. Chem. Int. Ed. 57 (2018) 5301–5305.
[32] E. Markevich, G. Salitra, F. Chesneau, M. Schmidt, D. Aurbach, Very stable lithium metal stripping–plating at a high rate and high areal capacity in fluoroethylene carbonate-based organic electrolyte solution, ACS Energy Lett. 2 (2017) 1321–1326.
[33] Y. Zhao, D. Wang, Y. Gao, T. Chen, Q. Huang, D. Wang, Stable Li metal anode by a polyvinyl alcohol protection layer via modifying solid-electrolyte interphase layer, Nano Energy 64 (2019), 103893.
[34] A. Masias, N. Felten, R. Garcia-Mendez, J. Wolfenstine, J. Sakamoto, Elastic, plastic, and creep mechanical properties of lithium metal, J. Mater. Sci. 54 (2019) 2585–2600.
[35] X. Shen, R. Zhang, X. Chen, X.B. Cheng, X.Y. Li, Q. Zhang, The failure of solid electrolyte interphase on Li metal anode: structural uniformity or mechanical strength, Adv. Energy Mater. 10 (2020), 1903645.
[36] Y. Lee, T.K. Lee, S. Kim, J. Lee, Y. Ahn, K. Kim, H. Ma, G. Park, S.M. Lee, S.K. Kwak, N.S. Choi, Fluorine-incorporated interface enhances cycling stability of lithium metal batteries with Ni-rich NCM cathodes, Nano Energy 67 (2020), 104309.
[37] Q. Liu, D. Mu, B. Wu, H. Xu, L. Wang, L. Gai, L. Shi, F. Wu, Theoretical studies of the reduction of cyclic esters on the anode interface of lithium batteries, J. Electrochem. Soc. 164 (2017) A3144–A3153.
[38] Y. Zhang, D. Krishnamurthy, V. Viswanathan, Engineering solid electrolyte interphase composition by assessing decomposition pathways of fluorinated organic solvents in lithium metal batteries, J. Electrochem. Soc. 167 (2020), 070554.
[39] L. Liu, S. Gu, S. Wang, X. Zhang, S. Chen, A $LiPO_2F_2$/$LiPF_6$ dual-salt electrolyte enabled stable cycling performance of nickel-rich lithium ion batteries, RSC Adv. 10 (2020) 1704–1710.
[40] W. Huang, H. Wang, D.T. Boyle, Y. Li, Y. Cui, Resolving nanoscopic and mesoscopic heterogeneity of fluorinated species in battery solid-electrolyte interphases by cryogenic electron microscopy, ACS Energy Lett. 5 (2020) 1128–1135.
[41] B.D. Adams, J. Zheng, X. Ren, W. Xu, J.G. Zhang, Accurate determination of coulombic efficiency for lithium metal anodes and lithium metal batteries, Adv. Energy Mater. 8 (2018), 1702097.
[42] W. Xue, Z. Shi, M. Huang, S. Feng, C. Wang, F. Wang, J. Lopez, B. Qiao, G. Xu, W. Zhang, Y. Dong, R. Gao, S.H. Yang, J.A. Johnson, J. Li, FSI-inspired solvent and "full fluorosulfonyl" electrolyte for 4 V class lithium-metal batteries, Energy Environ. Sci. 13 (2020) 212–220.

Shouyi Yuan is a Ph.D candidate under the supervision of Prof. Xia at the department of Chemistry, Fudan University. He received his master degree from Fudan university in 2016. His research interests focus on high-energy-density rechargeable batteries including lithium sulfur batteries, lithium metal anode, Li-O_2 batteries, aqueous zinc-ion batteries *et al.* He has published several papers including *Energy Environmental Science, Advanced Energy Materials, Nano Energy, Advancced Science et al.*

Suting Weng received her Bachelor's degree from Central South University in 2018. She is a PhD candidate in Institute of Physics, Chinese Academy of Sciences. Her research interests focus on the characterization of structural evolution and reaction mechanism of energy-storage materials by cryogenic electron microscopies (Cryo- EM).

Fei Wang is a professor at the Department of Materials Science, Fudan University. He received his Ph.D from Fudan University in 2015 under the supervision of Prof. Yongyao Xia. Before he joined Fudan University as professor, he worked as a postdoctoral fellow in Maryland University under the supervision of Prof. Chunsheng Wang and in MIT under the supervisions of Prof. Chiang Yet-Ming. His research interests focus on the advanced electrolytes for batteries and solid state batteries. He has published several papers including Science, Nature Materials et al.

Xiaoli Dong is an associate professor at the Department of Chemistry, Fudan University. She received her Ph.D. from Fudan University in 2017 supervised by Prof. Yong-Yao Xia. Her research mainly focuses on the novel electrolytes and electrode materials for low temperature applications, including lithium-ion batteries, sodium-ion batteries, electrochemical capacitors, and new devices.

Yonggang Wang received his Ph.D. in Physical Chemistry from Fudan University in 2007. From 2007 to 2011, he worked as a Post-doctoral Research Associate at the National Institute of Advanced Industrial Science and Technology (AIST), Japan. He is currently a full professor at the Department of Chemistry at Fudan University, China. His research interests include electrochemical functional materials and their application in lithium-ion batteries, metal-air batteries, aqueous batteries, supercapacitors, and fuel cells.

Cai Shen received his Ph.D. in Chemistry from the University of St Andrews at UK in 2008. Before joining Ningbo institute of Materials Technology and Engineering, Chinese Academy of Science (NIMTE) as an Associate Professor, he worked as a postdoc fellow in the University of Maryland (USA) and Aarhus University (Denmark). He has published more than 90 papers in peer-review journals. His current research interests are lithium-ion batteries and atomic force microscopy.

Prof. Junwei Lucas Bao obtained his Ph.D. in theoretical chemistry in 2018 at the University of Minnesota, Twin Cities, under the supervision of Prof. Donald Truhlar. He then went to Princeton University for a postdoctoral position in Prof. Emily Carter's group. In 2020, Lucas Bao joined the department of chemistry at Boston College and started his independent career. His research group focuses on using quantum mechanics, statistical mechanics and solid-state physics to understand atmospheric chemical kinetics, model clean-energy-driven catalysis, and design new materials. His group also works on developing new electronic-structure methods and kinetics/dynamics theories.

Xuefeng Wang is an Associate Professor in Institute of Physics, Chinese Academy of Sciences. He received his PhD from the Institute of Physics, Chinese Academy of Sciences in 2015, after which he worked as a postdoc research fellow in University of California San Diego. His research interest includes structural and mechanism exploration on energy-storage materials by cryogenic electron microscopies (Cryo- EM) and other advanced techniques including Li-ion batteries, Li metal, solid-state batteries, Li−O_2, and other metal batteries.

Yongyao Xia is a professor in the Department of Chemistry and Institute of New Energy of Fudan University. He received a Bachelor of Science degree from the Chemistry Department of Zhejiang Normal University in 1987 and a Master of Science degree in Electrochemistry from the Chemistry Department of Jilin University in 1990. He received a Ph.D. degree in Energy-Related-Material Science in Saga University, Japan in 1997. His research interests involve advanced materials and technologies for energy storage and conversion devices, e.g., lithium-ion batteries, sodium-ion batteries, electrochemical super-capacitors, lithium-air, lithium-sulfur batteries, etc.